Longitudinal variation of thermospheric density around the terminator from APOD

Guangming Chen[1] , Jiyao Xu[2], Xie Li[1], Maosheng He[3], Shushi Liu[1], Haijun Man[1], Hong Gao[2], Yongping Li[4]

1. Science and Technology on Aerospace Flight Dynamics Laboratory, Beijing Aerospace Control Center, Beijing, 100094, China

2. State Key Laboratory of Space Weather, National Space Science Center, Chinese Academy of Sciences, Beijing, 100190, China

3. Private, Kühlungsborn, Germany

4. Beijing Key Laboratory of Space Environment Exploration, National Space Science Center, Chinese Academy of Sciences, Beijing 100190, China

Corresponding author: Guangming Chen (chen_g_m@126.com)

Key Points:

- The longitudinal variation of thermospheric density around the terminator from APOD is extracted and compared with the NRLMSIS 2.0 predictions.
- The maximum of relative longitudinal variation is located near the geomagnetic pole, especially in the winter hemisphere.
- The maximum of relative longitudinal variation at dusk appears at a higher latitude with a larger value at dusk than at dawn in most months.

Abstract

This study presents the longitudinal distribution of thermospheric density around the terminator (in the dawn and dusk sectors), using observations collected by the atmospheric density detector onboard the Chinese satellite APOD (Atmospheric density detection and Precise Orbit Determination) from 2017 to 2018. The APOD observations show a significant relative longitudinal variation of thermospheric density with global maxima ($\Delta\rho_{rmax}$) near the geomagnetic pole, especially in the winter hemisphere. The annual maximum of $\Delta\rho_{rmax}$ appears in the Southern Hemisphere around the June solstices and reaches 26.3% and 39.6% at dawn and dusk, respectively. Compared with at dawn, $\Delta\rho_{rmax}$ occurs at a higher latitude with a larger value at dusk. The auroral heating and meridional wind might play an important role in the longitudinal variation of thermospheric density. We further compare the APOD observations with the NRLMSIS 2.0 model predictions under low solar activity condition. The NRLMSIS 2.0 model reproduces similar longitudinal variations to the observations, with hemispheric asymmetry and local time difference.

Plain Language Summary

The longitudinal distribution of upper atmospheric density has been broadly studied. However, the studies mostly focused on 24 h averaged distiribution. The paper presents the longitudinal distribution of upper atmospheric density around the terminator using observations collected by the Atmospheric Density Detector onboard the Chinese satellite APOD (Atmospheric density detection Precise Orbit Determination). The longitudinal distribution between dawn and dusk is compared and the seasonal variation is analyzed. The APOD observations show a significant relative longitudinal variation of thermospheric density with global maxima near the geomagnetic pole, especially in the winter hemisphere. The maximum of relative longitudinal variation at dusk appears at a higher latitude with a larger value at dusk than at dawn in most months. A comparison of the observations with the NRLMSIS 2.0 model predictions around the terminator is given. The study is beneficial for improving understanding of the upper atmosphere and facilitating the spacecraft orbit prediction.

Keywords: Thermospheric density, Longitudinal distribution, Dawn, Dusk, APOD, MSIS

1. Introduction

Variations of upper thermospheric density can cause perturbations in spacecraft orbits [e.g., Chen et al., 2012, 2014]. Thus, the variations under different geophysical conditions have attracted broad interest [e.g., Liu et al, 2005; Qian and Solomon, 2012]. One of these variations is the longitude/UT variation of the thermospheric density. The magnetospheric energy deposition could induce thermospheric variations with longitude through the auroral precipitation and Joule heating. Observational studies were typically based on in-situ measurements collected by slowly-processing polar satellites in low Earth orbits which are subject to an inherent sampling limitation associated with the orbits. The orbits typically take several months to cover 24 h local time. Therefore, the results often entangle the local time variation with the seasonal variation. To conquer this problem, Xu et al. (2013) developed a method by averaging the data across multi-years. The method could produce 24 h averaged longitudinal variations in different seasons, but it is still challenging to study the longitudinal variations at different local times. Using the observations by a detector onboard a sun-synchronous satellite can avoid this problem and produce longitudinal distributions at fixed local times.

The longitudinal variations of thermospheric density at ~200 km at 1030 LT and 2230 LT were obtained from the SETA experiments with a nearly Sun-synchronous orbit (Forbes et al., 1999; Forbes et al., 2012). However, the longitudinal variations of upper thermospheric density are still rare above 300 km at fixed local times. It is important because most low-orbit spacecrafts fly through the upper thermosphere. Furthermore, the longitudinal variations around the terminator are unknown. Given that the horizontal gradient of solar radiation is prominent in the sectors, a large gradient of thermospheric density is also expected; therefore, the longitudinal distribution may differ from other local times [Liu et al., 2009]. The Chinese APOD satellite flies in a circular Sun-synchronous orbit carrying an Atmospheric Density Detector (ADD) and detects the thermospheric density around the terminator [Li et al., 2018; Tang et al., 2019; Calabia et al., 2020]. It allows us to study the longitudinal variations around the terminator in the upper thermosphere.

The current paper studies the longitudinal distributions of thermospheric density at 460km around the terminator using the measurements from the Chinese satellite APOD. In this work, we focus on answering the following two open questions: (1) What is the longitudinal variation of the thermospheric density at dawn and dusk in different seasons? (2) Does the longitudinal variation at dawn differ from at dusk?

2. Data and method

The Chinese APOD satellites, including APOD-A, -B, -C, and -D, were launched into a circular Sun-synchronous in 2015. Onboard APOD-A is an Atmospheric Density Detector (ADD), which samples the thermospheric density at a rate of 1 Hz, corresponding to a spatial resolution of ~8 km. This paper uses the thermospheric density observations only from APOD-A, and refers to APOD-A as APOD. The principle of the ADD and the data processing method were detailed by Li et al. [2018] and Tang et al. [2019]. The longitudinal distribution of thermospheric mass density is constructed using the observations under quiet geomagnetic conditions (Ap<10) in 2017 and 2018 when the Sun is at a low activity level with an annual

average of F10.7 index around 77 and 70, respectively.

The data observed are proceeded in its descending and ascending legs separately. These two legs cross the equator at the local time around 0730LT and 1930 LT and hereinafter are referred to as dawn and dusk sectors. To exclude the altitude and local time variations associated with the APOD orbit, we normalized the mass densities using the NRLMSIS 2.0 model [Emmert et al., 2021] to fixed reference heights of 460 km [Liu et al., 2005; Ma et al., 2010] at local time 0730 LT and 1930 LT, respectively. In each sector and in each month, the data are binned in grids of 5° in latitude and 20° in longitude from 82.5°S to 82.5°N. Figure 1, as an example, displays a histogram of the data collected in July. The histogram indicates that the observations are sufficiently at all given grids, allowing reliable statistics.

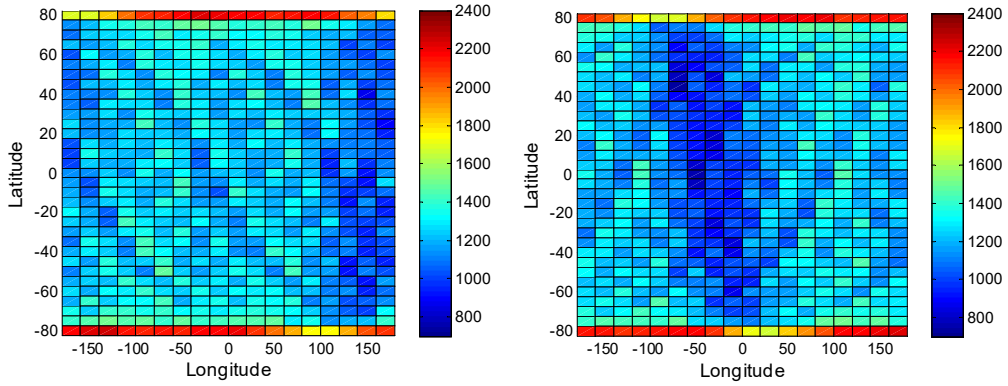

Figure 1. Global distributions of the samplings from APOD at dawn (left) and dusk (right) in July.

The monthly averaged APOD density (ρ)is calculated in each grid at dawn or at dusk, respectively. Then Equation (1) is used to obtain the zonal mean of the monthly averaged thermospheric density ($\bar{\rho}$),

$$\bar{\rho} = \frac{1}{2\pi}\int_0^{2\pi} \rho \mathrm{d}\lambda \quad (1),$$

where λ denotes longitude.

Equation (2) is used to estimate the relative longitudinal variation of thermospheric density,

$$\Delta\rho_r = \rho / \bar{\rho} - 1 \quad (2).$$

3. Results and Discussion

Figures 2 and 3 show the global distributions of relative longitudinal variation ($\Delta\rho_r$) from APOD in different months at dawn and dusk, respectively. The most prominent feature is that there is one region with high $\Delta\rho_r$ in each hemisphere. The maximum of $\Delta\rho_r$ ($\Delta\rho_{rmax}$) appears at 60°W - 120°W in longitude in the northern hemisphere and at 100°E -180°E in longitude in the Southern Hemisphere. From November to February, the high-density region

in the northern hemisphere is more pronounced. The global $\Delta\rho_{rmax}$ appear at 65°N - 75°N in latitude and 60°W - 120°W in longitude. From April to September, the high-density region in the Southern Hemisphere is more pronounced and $\Delta\rho_{rmax}$ is located at 50°S - 75°S and 100°E - 180°E. The location of $\Delta\rho_{rmax}$ is close to the geomagnetic pole, which was at (~83°N, ~84°W) in the northern hemisphere and (~75°S, ~125°E) in the Southern Hemisphere in 2017-2018 according to the altitude adjusted corrected geomagnetic (AACGM) coordinates [Shepherd, 2014]. It is known that the aurora heating is mainly around the geomagnetic pole [e.g., Pulkkinen et al., 2011; Gao et al., 2020; Yu et al., 2021]. The aurora heating can cause the enhancement of temperature in the lower thermosphere [e.g., Xu et al. 2013b] and themospheric density in the upper thermosphere [e.g., Wang et al., 2021]. Thus the maximum of $\Delta\rho_r$ occurring near the geomagnetic pole can be attributed to the aurora heating, including the aurora particles precipitation and Joule heating.

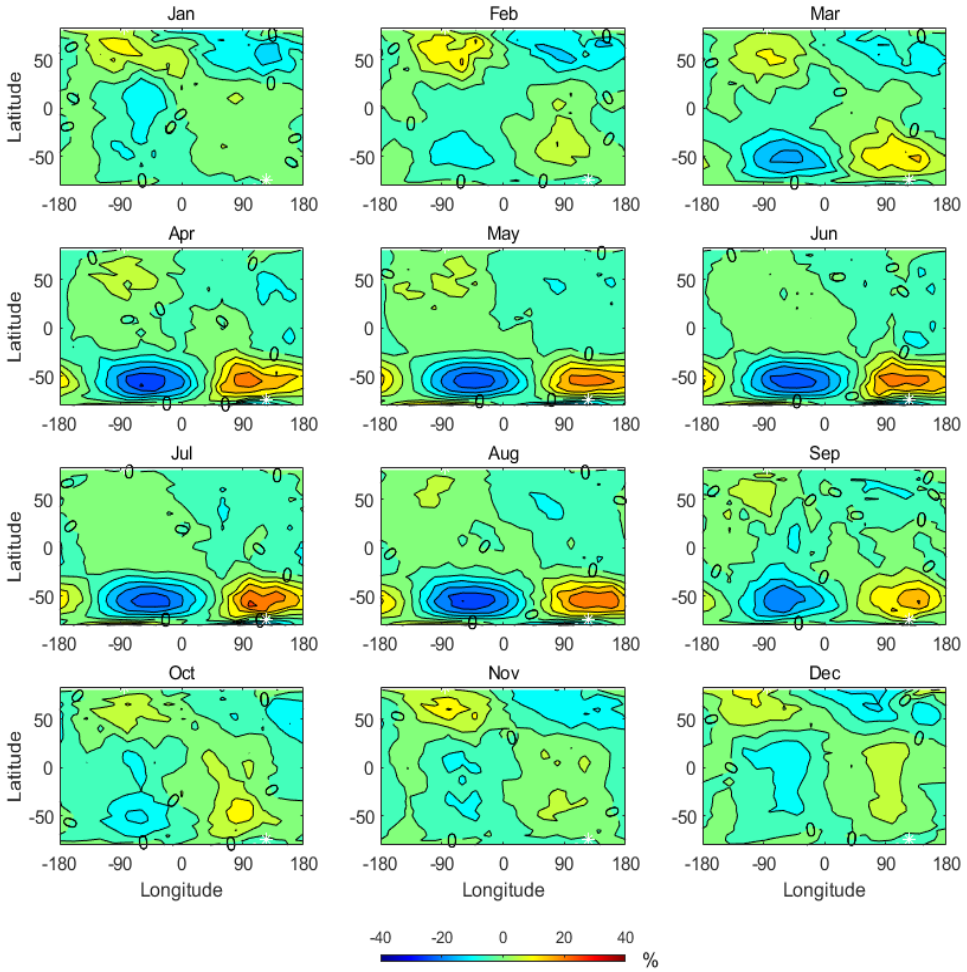

Figure 2. The global distributions of the relative longitudinal variation ($\Delta\rho_r$) from APOD at 0730 LT (dawn) in different months. White stars denote the position of the south geomagnetic pole.

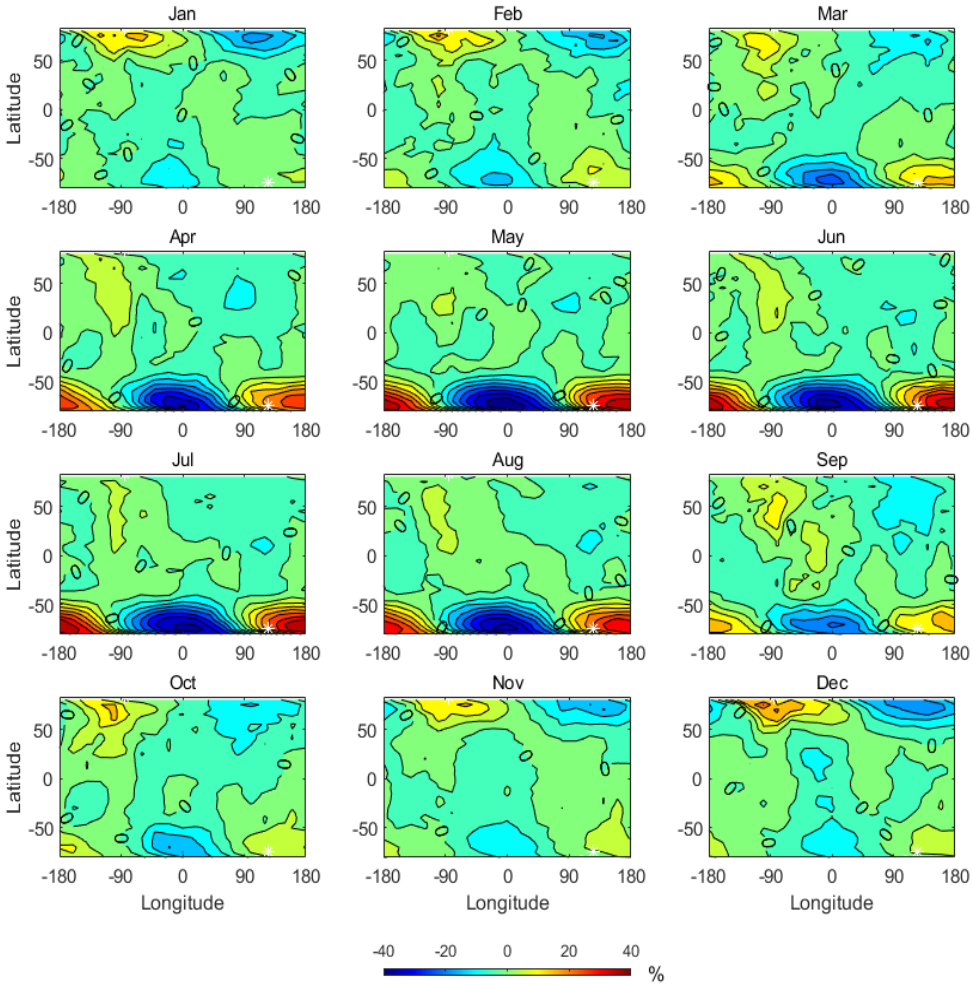

Figure 3. Same as Figure 2 but for the thermospheric densities at 1930 LT (dusk).

In Figures 2 and 3, the maxima of $\Delta\rho_r$ in the Southern Hemisphere are greater than in the northern hemisphere at both dawn and dusk from April to August. While, from November to February, the maxima of $\Delta\rho_r$ in the northern hemisphere is greater than in the Southern Hemisphere which is in summer. For example, in December, the maxima of $\Delta\rho_r$ in the northern hemisphere is 13.2% and 25.4% at dawn and dusk, respectively, while the maxima in the Southern Hemisphere are only 9.0% and 7.1% at dawn and dusk,, respectively. It indicates that $\Delta\rho_{rmax}$ in the winter hemisphere is higher than in the summer hemisphere around the solstices. The difference of $\Delta\rho_{rmax}$ between the summer and winter hemispheres may be caused by the difference in the solar EUV energy input into the thermosphere between two hemispheres. At the same latitude in two hemispheres, the solar elevating angle in the winter hemisphere is smaller than in the summer and some polar regions in the winter hemisphere are not even lit by the Sun. Therefore, the EUV energy input into the thermospheric atmosphere and $\bar{\rho}$ in the winter hemisphere are much less than those in the summer hemisphere, which causes the lower background thermosphere density in the winter

158 hemisphere. According to Eq.(2), $\Delta\rho_r$ is inversely proportional to the value of $\bar{\rho}$. Thus $\Delta\rho_{rmax}$
159 caused by the auroral heating in the winter hemisphere was more siginifcantly than in the
160 summer hemisphere.

161 It can be seen in Figures 2 and 3 that the annual maxima of $\Delta\rho_{rmax}$ in the Southern
162 Hemisphere appear near the geomagnetic pole (~75°S, ~125°E) in July at dawn and dusk.
163 The values reach 26.3% and 39.6%, respectively. The annual maxima of $\Delta\rho_{rmax}$ in the
164 northern hemisphere appear in February and December at dawn and dusk, with the values of
165 15.8% and 25.4%, respectively. The annual maxima of $\Delta\rho_{rmax}$ in the Southern Hemisphere are
166 much greater than in the northern hemisphere. The difference of $\Delta\rho_{rmax}$ between the two
167 hemispheres should be mainly caused by the different geomagnetic pole positions relative to
168 the geographic poles. Since the aurora heating is mainly around the geomagnetic pole
169 [Pulkkinen et al., 2011; Gao et al., 2020] and the southern geomagnetic pole is further off the
170 geographical pole, the effects of auroral heating on the thermosphere in the Southern
171 Hemisphere are harder to cover all longitudes. Thus, the longitudinal variation of
172 thermospheric density in the Southern Hemisphere should be relatively stronger in the
173 Northern Hemisphere under the same other conditions. Xu et al. [2013a] analyzed the
174 longitudinal variation of thermospheric density using the CHAMP and GRACE satellite
175 observations. Their results showed that the maximal longitudinal variations averaged for all
176 local times also appear near the geomagnetic poles. Similar to the APOD observations, the
177 CHAMP and GRACE satellite observations showed an apparent hemispheric asymmetry in
178 the longitudinal structure, being more pronounced in the Southern Hemisphere than in the
179 Northern Hemisphere. To sum up, the main feature of the global distribution around the
180 terminator from APOD is similar to the distriubition averged over all local times from
181 GRACE.

182 As is shown in Figures 2 and 3, the longitudinal variations of $\Delta\rho_r$ around the
183 geomagnetic pole significantly expand to the middle and low latitudes. The expansion
184 diminishes with latitude decreasing, and the values of $\Delta\rho_r$ at low latitudes vary between -10%
185 and 10% in most months. The expansion also changes with the seasons. Near the solstices,
186 the longitudinal variation around the geomagnetic pole in the summer hemisphere not only
187 can control the low latitudes, but also can extend to the other hemisphere. Otherwise, the
188 longitudinal variations around the geomagnetic pole in the winter hemisphere have weaker
189 impacts on the mid-low latitudes, although the maxima of $\Delta\rho_r$ in the winter hemisphere are
190 larger. The difference in equatorward expansion could be related to the meridional wind in
191 the mid-low latitudes. To clarify the contribution of meridional wind to the equatorward
192 expansion and the asymmetry of $\Delta\rho_{rmax}$ between two hemispheres, the meridional wind in the
193 middle and high latitudes at dawn (0730 LT) and at dusk (1930 LT) is calculated according to
194 the HL-TWiM empirical model, which synthesizes extensive collection of historical
195 high-latitude wind measurements and presents a good characterization of the high-latitude
196 neutral winds in geomagnetic coordinates at altitudes between 210 and 320 km [Dhadly et al.,
197 2019]. The seasonal distribution of meridional wind between 30°N - 80°N at 84°W and 30°S
198 - 80°S at 125°E is given in the upper panel of Figure 4. According to Figure 4, during the
199 solstices, the prevailing meridional wind in the themosphere is equatorward in the summer
200 hemisphere and poleward at 30° - 40° in the winter hemisphere. The equatorward wind

should be helpful for the longitudinal variations of $\Delta\rho_{rmax}$ around the magnetic pole in the summer hemisphere extending to low latitudes, even to the other hemisphere, and may help reduce the value of $\Delta\rho_{rmax}$ in the summer hemisphere.

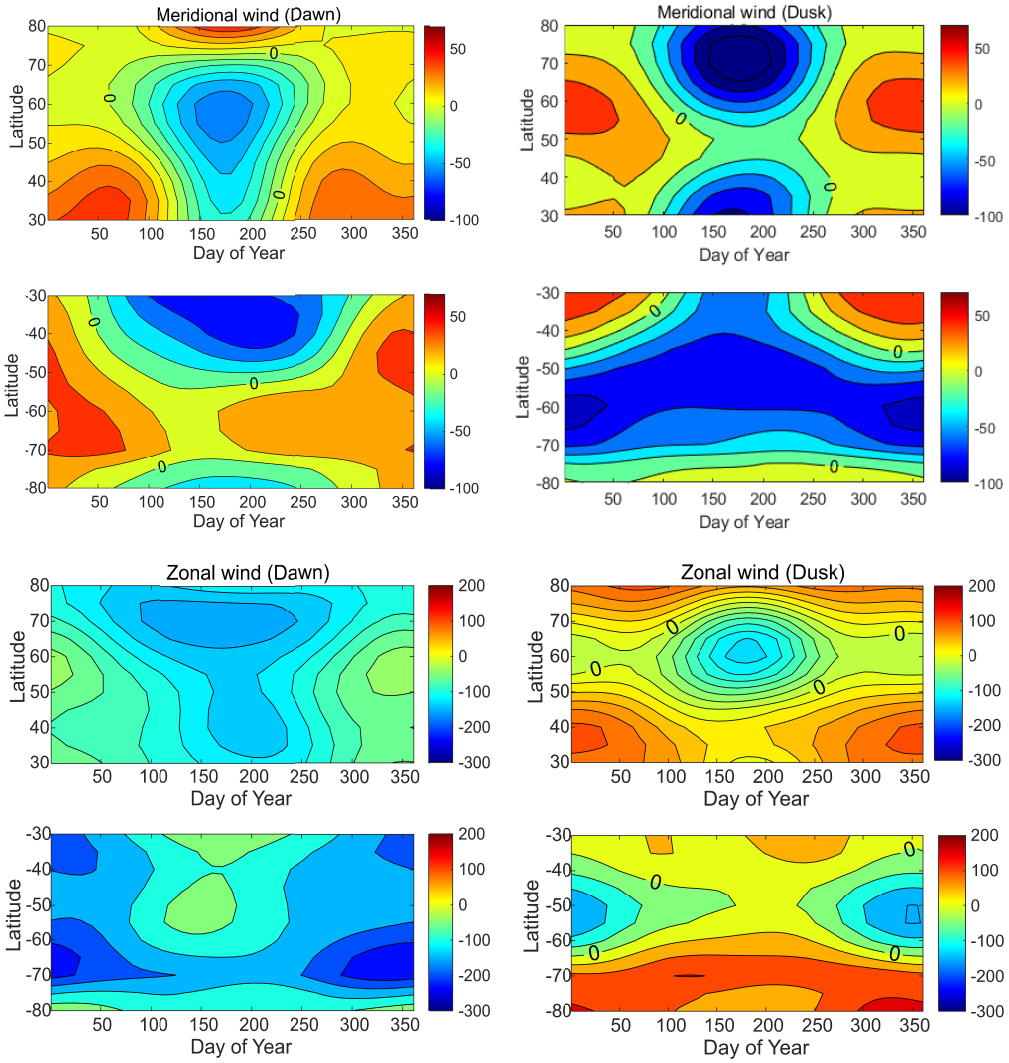

Figure 4. The latitudinal and seasonal variations of meridional (upper) and zonal (lower) wind at altitudes between 210 and 320 km at 0730LT (left) and 1930LT (right) from the HL-TWiM model.

Figures 2 and 3 show that $\Delta\rho_{rmax}$ from APOD appears at (50°S - 60°S, 80°E-140°E) at dawn and (70°S -75°S, ~180°E) at dusk from April to August. The global $\Delta\rho_{rmax}$ appears at (65°N - 75°N, 60°W-120°W) at dawn and at (~75°N, 60°W-100°W) at dusk from November to February. Compaing the latitudes of $\Delta\rho_{rmax}$ at dawn and dusk, the latitudes of $\Delta\rho_{rmax}$ at dusk are higher and closer to the geomagnetic pole in two hemispheres. According to the longitudes of $\Delta\rho_{rmax}$, the positions of $\Delta\rho_{rmax}$ at dusk are in the east of that at dawn, especially in the southern hemisphere. The difference between the latitudes where $\Delta\rho_{rmax}$ appears at dawn and at dusk may be related to the meridional wind. According to the results from the HL-TWiM empirical model in the upper panel in Figure 4, the mid-high latitude thermospheric wind is poleward and maxima at 50°S with a value of -76ms^{-1} at dusk. At

dawn, it is equatorward or poleward with lower values relative to that at dusk between 50°S and 75°S. Take December as an example. The thermospheric meridional wind between 50°N and 75°N is less than 15 ms^{-1} at dawn. It is polarward and has larger values at dusk. The largest meridional wind speed reaches above 50 ms^{-1}, around 60°N at dusk. More intensive poleward wind might induce the location of $\Delta\rho_{rmax}$ extending to the polar region at dusk. In addition, the difference in longitudes where $\Delta\rho_{rmax}$ appears at dawn and at dusk could be attributed to the zonal wind. From the lower pannel of Figure 4, the zonal wind at the latitude where $\Delta\rho_{rmax}$ appears is westward in the two hemispheres at dawn. The westward wind should help $\Delta\rho_{rmax}$ extending westwardly at dawn. At dusk, the zonal wind at the latitude where $\Delta\rho_{rmax}$ appears is eastward in two hemispheres. The eastward wind should help $\Delta\rho_{rmax}$ extending eastwardly at dusk. The different zonal wind could explain the difference in the longitude where $\Delta\rho_{rmax}$ appears at dawn and at dusk. The zonal wind in the southern hemisphere reaches more than 70 ms^{-1}, which is larger than in the Northern Hemisphere. Thus the difference in the longitude where $\Delta\rho_{rmax}$ appears between dawn and dusk is pronounced in the Southern Hemisphere. The exact reason may need further study through additional observation and numerical simulation.

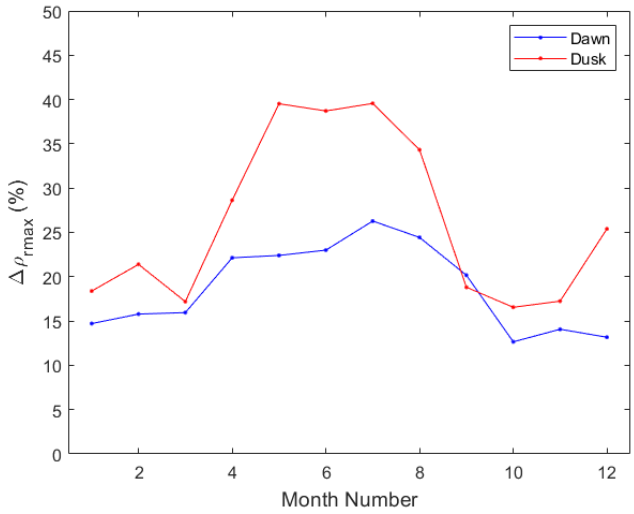

Figure 5. Seasonal variation of $\Delta\rho_{rmax}$ at dawn and dusk from APOD. The blue and red lines denote the dawn and dusk sectors.

Figure 5 shows the seasonal variation of $\Delta\rho_{rmax}$ from APOD at dawn and dusk. The annual maxima of $\Delta\rho_{rmax}$ from APOD occur in July at both dawn and at dusk. Xu et al. [2013a] showed that the annual maxima of $\Delta\rho_{rmax}$ from the GRACE observations occurred during equinoxes. The difference in peak occurrence time may be due to the different solar activity levels and local times. The results in Xu et al. [2013a] are averaged over all local times at the high, middle, and low solar activity levels. The results from APOD in the paper are only for around the terminator at low solar activity level. Xu et al. [2014] and Shreedevit et al. [2019] showed that the seasonal variation of ionospheric density at the high latitudes in the Southern Hemisphere has significant solar activity and localtime dependence. Their results showed that the ionospheric density at the high latitudes of the Southern Hemisphere usually has semiannual anomaly with peaks during the equinoxes for high and middle solar activity conditions, especially during the daytime. The larger ionospheric density may produce larger

conductivity and Joule heating during the equinoxes. This could cause that GRACE's largest longitudinal variations of theromospheric density occur during the equinoxes. It has been reported that the ionospheric density at the high latitudes in the Southern Hemisphere has no significant semiannual anomaly and has a relatively low value during the equinoxes under low solar activity conditions [e.g., Qian et al, 2013; Xu et al., 2014; Shreedevit et al., 2019]. Thus the $\Delta\rho_{rmax}$ from APOD in this paper has no significant peaks during the equinoxes.

Figure 5 shows that the annual maxima of $\Delta\rho_{rmax}$ from APOD reach 26.3% and 39.6% at dawn and dusk in July, respectively. It can also be seen from Fig. 2 and Fig. 3. However, the annual maxima of $\Delta\rho_{rmax}$ at 480 km from GRACE was only 15.2% [Xu et al., 2013a]. It is much less than the corresponding values of 26.3% at dawn or 39.6% at dusk from APOD. The results from the GRACE observation in Xu et al. [2013a] are for all local times. According to the above results at dawn and dusk from APOD (see Figures 2 and 3), there are significant differences in the peak locations for different local times. So the maxima of averaged $\Delta\rho_r$ for the two local times could be less than $\Delta\rho_{rmax}$ at dawn or at dusk. If all the observations at both dawn and dusk from APOD are used together to obtain the mean relative longitudinal variation around the terminator, the maximum will be ~24%, which is more closer to the maximum from the GRACE data. So the different locations of $\Delta\rho_{rmax}$ at different local times could bring the lower values of $\Delta\rho_{rmax}$ averaged for all local times. Furthermore, the data observed from 2017 to 2018 and 5° latitude×1 month bins are used in this work, while the data from 2003 to 2008 and 10° latitude×2 month bins were used in Xu et al. [2013a]. The different time periods and bins used can also contribute to the different results. In addition, the difference in $\Delta\rho_{rmax}$ may also be due to the different solar activity levels in different years.

Figure 5 shows that $\Delta\rho_{rmax}$ from APOD at dusk is significantly greater than at dawn in most months. For example, $\Delta\rho_{rmax}$ in June reaches 23.0% and 38.7% at dawn and at dusk, respectively. The difference in $\Delta\rho_{rmax}$ between at dawn and at dusk maybe related to their different latitudes. From above, we know that $\Delta\rho_{rmax}$ is located at a higher latitude at dusk than at dawn around the solstices. Since a degree in longitude at a higher latitude represents a shorter length, the area of a higher density region should be larger at dawn than that at dusk. The larger area of the higher density region should contribute to the lower $\Delta\rho_{rmax}$ at dawn. The observations from CHAMP in Yamazaki et al. [2015] also show that the high-latitude density response is least significant around the dawn sector in both hemispheres.

Predictions of spacecraft orbits are often subject to the uncertainty of the atmospheric semi-empirical models [Emmert et al., 2017]. The semi-empirical model series of Mass Spectrometer Incoherent Scatter Radar (MSIS) [*Picone et al.*, 2002, and Liu et al., 2017] are widely used in the thermospheric research and aerospace engineering and have been upgraded to the new version as NRLMSIS 2.0 (Emmet et al., 2021). Herein, NRLMSIS 2.0 is shortened to "MSIS 2.0" for brevity. We compare the APOD measurements with the MSIS 2.0 model predictions. Figures 6 and 7 show the longitudinal variations of thermospheric density ($\Delta\rho r$) from the MSIS 2.0 model at 460 km at dawn and dusk, respectively. Similar to the APOD data, the MSIS 2.0 predictions exhibit one zonal peak near the geomagnetic pole in the northern and southern hemispheres. The annual maxima of $\Delta\rho_{rmax}$ in the southern hemisphere at dawn and dusk from MSIS 2.0 appear in August with values of 28.8% and 34.7%, respectively. The annual maximum of $\Delta\rho_{rmax}$ in the Northern Hemisphere from MSIS

2.0 occur between December and February, and both values are ~14%. They are slightly less than the annual maxima from APOD. Figures 6 and 7 show that $\Delta\rho_{rmax}$ from MSIS 2.0 in the Southern Hemisphere is larger than those in the northern hemisphere at dawn and dusk from March to September. The annual maximum of $\Delta\rho_{rmax}$ appears in the Southern Hemisphere. It is the same as the results from APOD. There are some differences between $\Delta\rho_{rmax}$ from APOD and MSIS 2.0. From November to February, $\Delta\rho_{rmax}$ from MSIS 2.0 in the Southern Hemisphere is larger, while $\Delta\rho_{rmax}$ from APOD in the northern hemisphere is larger. Take December as an example. In December, $\Delta\rho_{rmax}$ in the northern hemisphere from APOD is 13.2% and 25.4% at dawn and dusk, respectively. $\Delta\rho_{rmax}$ from MSIS 2.0 is only 9.0% and 14.3%, respectively. In the Southern Hemisphere, $\Delta\rho_{rmax}$ from APOD in December is just 9.0% and 7.1% at dawn and at dusk, respectively. $\Delta\rho_{rmax}$ from the MSIS 2.0 model is 13.4% and 18.8%, respectively. Thus, $\Delta\rho_{rmax}$ from MSIS 2.0 appear in the Southern Hemisphere in all months. Correspondingly, $\Delta\rho_{rmax}$ from APOD appears in the Southern Hemisphere near the equinoxes and in the winter hemisphere around the solstices. The MSIS 2.0 model might overestimate the longitudinal variations of thermospheric density in the Southern Hemisphere and underestimate them in the northern hemisphere around the December solstice for low solar activity conditions. The structure of longitudinal variation in the series of MSIS models is the averaged results from the measurements of several satellites, especially the Dynamics Explorer-B satellite, which flied in an Elliptical orbit near solar maximum [Hedin, 1987; Picone et al., 2002; Emmet et al., 2021].

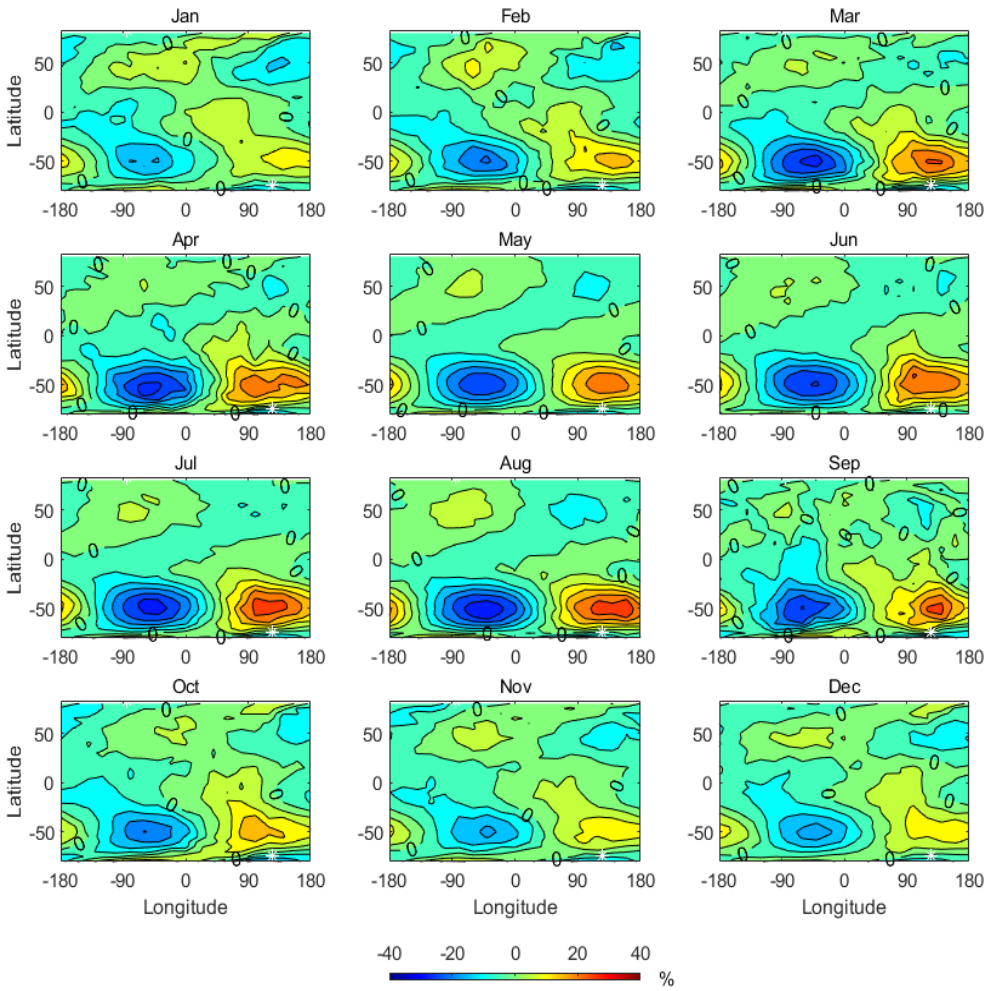

Figure 6. Same as Figure 2 but for the MSIS 2.0 model predictions.

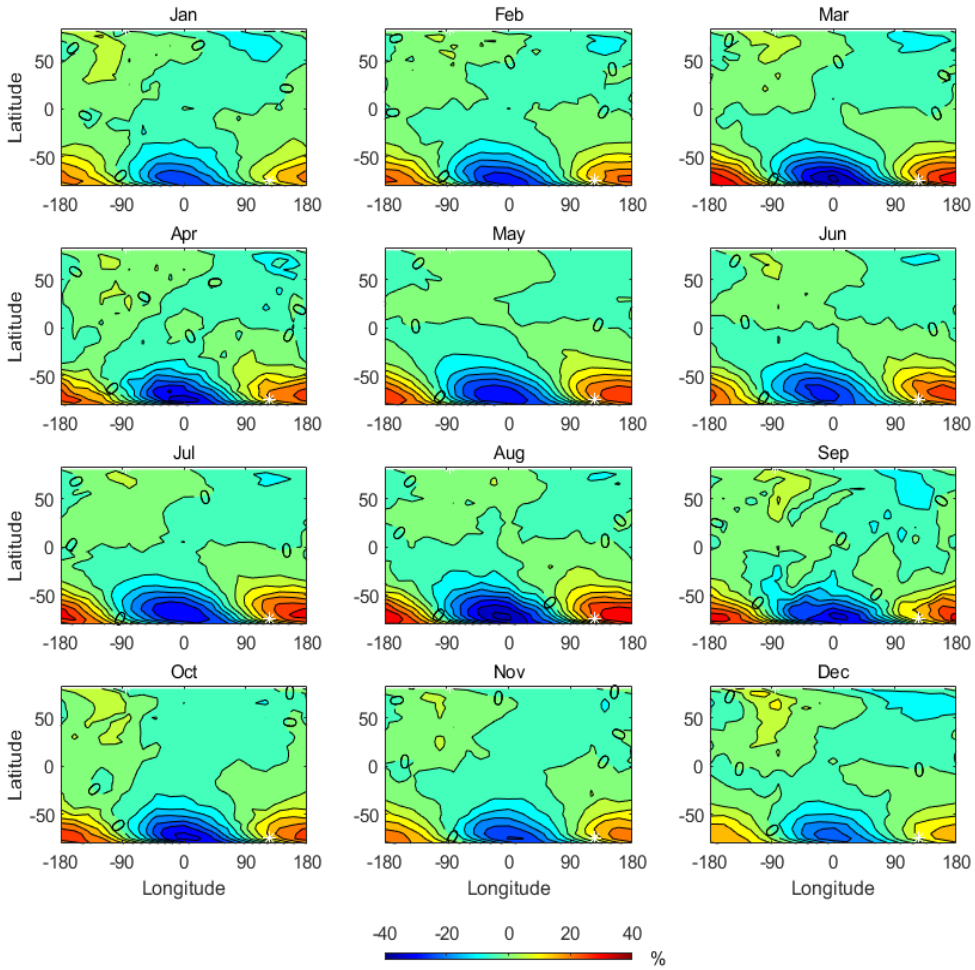

Figure 7. Same as Figure 3 but for the MSIS 2.0 model predictions.

As described above, the comparison of the APOD density between at dusk and at dawn indicates that $\Delta\rho_{rmax}$ at dusk from APOD is located at a higher latitude with larger values than at dawn. It can be seen in Figures 6 and 7 that the MSIS 2.0 results have the same characteristics. $\Delta\rho_{rmax}$ from MSIS 2.0 is located at 45°S - 50°S and 45°N - 60°N at dawn, and located at 70°S - 75°S and 60°N - 75°N at dusk. It is the same as the observations in two hemispheres from APOD that $\Delta\rho_{rmax}$ from MSIS at dusk is located at a higher latitude relative to that at dawn. In addition, it can be seen that the value of $\Delta\rho_{rmax}$ from MSIS 2.0 is also more pronounced at dusk than at dawn, similar to the result from APOD. For example, $\Delta\rho_{rmax}$ from the MSIS 2.0 mode0l in August is 28.8% and 34.7% at dawn and dusk, respectively. Meanwhile,, there is some difference in the annual variation of $\Delta\rho_{rmax}$ from APOD and that from MSIS. At dusk, the annual maxima of $\Delta\rho_{rmax}$ from APOD and from MSIS occur in July and in August, respectively. There is another peak of $\Delta\rho_{rmax}$ from MSIS with a value of 34.1% in March. There is no peak of $\Delta\rho_{rmax}$ from APOD in March and the value is only 17.2%.

3 Summary

The paper focuses on the longitudinal distributions of upper thermospheric density around the solar terminator under quiet geomagnetic conditions at low solar activity levels

using the Atmospheric Density Detector (ADD) observations aboard the APOD satellite. The measurements from ADD/APOD are compared with the MSIS 2.0 model predictions. The APOD observations show a significant longitudinal variation of thermospheric density with maxima near the geomagnetic pole, especially in the winter hemisphere. The longitudinal distribution around the terminator is similar to the average distriubition for all local time in general, but with a larger maximum of $\Delta\rho_{rmax}$. The annual maxima of $\Delta\rho_{rmax}$ appear in the Southern Hemisphere around the July solstices. The values of maxima at dawn and dusk reach 26.3% and 39.6%, respectively. In most months of the year, $\Delta\rho_{rmax}$ at dusk for APOD is located at a higher latitude with larger values than at dawn. The auroral heating and meridional wind might play an important role in the longitudinal variation of thermospheric density. In general, the relative longitudinal variations from the MSIS model density show good agreement with those from the observations. However, around the December solstice, the MSIS 2.0 model might overestimate the longitudinal variations in the Southern Hemisphere and underestimates them in the northern hemisphere.

Acknowledgment

This study was supported by the National Natural Science Foundation of China (41874183, 41474131 and 41604131). The authors also gratefully acknowledge use of the NRLMSIS 2.0 model and the HL-TWiM model. We thank Huixin Liu for the valuable remarks that helped to improve the original manuscript.

Open Research（Data Availability Statement）

The APOD data are provided by the Beijing Aerospace Control Center (ftp://36.110.27.60/product/APOD). NRLMSIS 2.0 Code used in this work are available at https://map.nrl.navy.mil/map/pub/nrl/NRLMSIS/NRLMSIS2.0. HL-TWiM Code used in this work is available at https://doi.org/10.5065/ad71-8827. F10.7 and *ap* indexes are available at NASA OMNIWeb data explorer (http://omniweb.gsfc.nasa.gov/form/dx1.html).

References

Calabia, A., Tang, G., & Jin, S. (2020), Assessment of new thermospheric mass density model using NRLMSISE-00 model, GRACE, Swarm-C, and APOD observations. *Journal of Atmospheric and Solar-Terrestrial Physics*, *199*, 105207, doi.org/10.1016/j.jastp.2020.105207.

Chen, G. M., Xu, J., Wang, W., Lei, J., & Burns, A. G. (2012), A comparison of the effects of CIR- and CME-induced geomagnetic activity on thermospheric densities and spacecraft orbits: Case studies. *Journal of Geophysical Research: Space Physics*, *117*(A8) , doi.org/10.1029/2012JA017782.

Chen, G. M., Xu, J., Wang, W., & Burns, A. G. (2014), A comparison of the effects of CIR- and CME-induced geomagnetic activity on thermospheric densities and spacecraft orbits: Statistical studies. *Journal of Geophysical Research: Space Physics*, *119*(9), 7928-7939, doi.org/10.1002/2014JA019831.

Dhadly, M. S., Emmert, J. T., Drob, D. P., Conde, M. G., Aruliah, A., Doornbos, E., et al.

(2019), HL−TWiM empirical model of high-latitude upper thermospheric winds. *Journal of Geophysical Research: Space Physics*, *124*(12), 10592-10618, doi.org/10.1029/2019JA027188.

Emmert, J. T., Warren, H. P., Segerman, A. M., Byers, J. M., & Picone, J. M. (2017), Propagation of atmospheric density errors to satellite orbits. *Advances in Space Research*, *59*(1), 147-165. , doi:10.1016/j.asr.2016.07.036.

Emmert, J. T., Drob, D. P., Picone, J. M., Siskind, D. E., Jones Jr, M., Mlynczak, M. G., ... & Yuan, T. (2021), NRLMSIS 2.0: A whole‐atmosphere empirical model of temperature and neutral species densities. *Earth and Space Science*, *8*(3), e2020EA001321.

Forbes, J. M., Palo, S. E., & Marcos, F. A. (1999), Longitudinal structures in lower thermosphere density. *Journal of Geophysical Research: Space Physics*, *104*(A3), 4373-4385.

Gao, H., Xu, J., Chen, G., Zhu, Y., Liu, W., & Wang, C. (2020), Statistical structure of nighttime O2 aurora from SABER and its dependence on geomagnetic and solar activities in winter. Journal of Geophysical Research: Space Physics, 125, e2020JA028302. https://doi.org/10.1029/2020JA028302

Hedin, A. E. (1987). MSIS‐86 thermospheric model. Journal of Geophysical Research: Space Physics, 92(A5), 4649-4662.

Li, X., Xu, J., Tang, G., Chen, G., Man, H., Liu, S., & Li, Y. (2018), Processing and calibrating of in-situ atmospheric densities for APOD. *Chinese Journal of Geophysics*, *61*(9), 3567-3576, doi: 10.6038/cjg2018L0452.

Liu, H., Lühr, H., Henize, V., & Köhler, W. (2005), Global distribution of the thermospheric total mass density derived from CHAMP. *Journal of Geophysical Research: Space Physics*, *110*(A4). A04301, doi:10.1029/2004JA010741.

Liu, H., Lühr, H., & Watanabe, S. (2007), Climatology of the equatorial thermospheric mass density anomaly. *Journal of Geophysical Research: Space Physics*, *112*(A5), A05305, doi:10.1029/2006JA012199.

Liu, H., Lühr, H., & Watanabe, S. (2009), A solar terminator wave in thermospheric wind and density simultaneously observed by CHAMP. *Geophysical Research Letters*, *36*(10), L10109, doi:10.1029/2009GL038165.

Liu, H., Thayer, J., Zhang, Y., & Lee, W. K. (2017), The non–storm time corrugated upper thermosphere: What is beyond MSIS?. *Space Weather*, *15*(6), 746-760, doi:10.1002/2017SW001618.

Ma, R., Xu, J., Wang, W., Lei, J., Liu, H. L., Maute, A., & Hagan, M. E. (2010), Variations of the nighttime thermospheric mass density at low and middle latitudes. *Journal of Geophysical Research: Space Physics*, *115*(A12), A12301, doi:10.1029/2010JA015784.

Picone, J. M., Hedin, A. E., Drob, D. P., & Aikin, A. C. (2002), NRLMSISE‐00 empirical model of the atmosphere: Statistical comparisons and scientific issues. *Journal of Geophysical Research: Space Physics*, *107*(A12), SIA-15, 1468, doi:10.1029/2002JA009430.

411 Pulkkinen, T. I., Tanskanen, E. I., Viljanen, A., Partamies, N., & Kauristie, K. (2011).
412 Auroral electrojets during deep solar minimum at the end of solar cycle 23. *Journal of*
413 *Geophysical Research: Space Physics*, 116(A4). doi: 10.1029/2010JA016098.

414 Qian, L., & Solomon S. (2012), Thermospheric Density: An Overview of Temporal and
415 Spatial Variations, *Space Sci. Rev.*, DOI 10.1007/s11214-011-9810-z.

416 Qian, L., Burns, A. G., Solomon, S. C., and Wang, W. (2013), Annual/semiannual
417 variation of the ionosphere, *Geophys. Res. Lett.*, 40, 1928– 1933, doi:10.1002/grl.50448.

418 Shepherd, S. G. (2014), Altitude‐adjusted corrected geomagnetic coordinates:
419 Definition and functional approximations. *Journal of Geophysical Research: Space*
420 *Physics*, *119*(9), 7501-7521, doi:10.1002/2014JA020264.

421 Shreedevit, P.R., Choudhary, R.K., Yu, Y., Thomas, E.G. (2019), Morphological study on
422 the ionospheric variability at Bharati, a polar cusp station in the southern hemisphere. *Journal*
423 *of Atmospheric and Solar-Terrestrial Physics*, doi: 10.1016/j.jastp.2019.105058.

424 Tang, G., Li, X., Cao, J., Liu, S., Chen, G., Man, H., et al. (2020), APOD mission status
425 and preliminary results. *Science China Earth Sciences*, *63*(2), 257-266.,
426 https://doi.org/10.1007/s11430-018-9362-6.

427 Wang, X., Miao, J., Lu, X., Aa, E., Liu, J., Wang, Y., & Liu, S. (2021). Latitudinal
428 impacts of Joule heating on the high-latitude thermospheric density enhancement during
429 geomagnetic storms. *Journal of Geophysical Research: Space Physics*, 126, e2020JA028747.
430 doi:10.1029/2020JA028747.

431 Weng, L., Lei, J., Doornbos, E., Fang, H., & Dou, X (2018), Seasonal variations of
432 thermospheric mass density at dawn/dusk from GOCE observations, *Ann. Geophys.*, 36(2),
433 489–496, https://doi.org/10.5194/angeo-36-489-2018.

434 Xu, J., Wang, W., & Gao, H. (2013), The longitudinal variation of the daily mean
435 thermospheric mass density. *Journal of Geophysical Research: Space Physics*, *118*(1),
436 515-523, doi:10.1029/2012JA017918.

437 Xu, J., Smith, A. K., Wang, W., Jiang, G., Yuan, W., Gao, H., et al. (2013), An
438 observational and theoretical study of the longitudinal variation in neutral temperature
439 induced by aurora heating in the lower thermosphere. *Journal of Geophysical Research:*
440 *Space Physics*, *118*(11), 7410-7425, doi:10.1002/2013JA019144.

441 Xu, S., Zhang, B. C., Liu, R. Y., Guo, L. X., & Wu, Y. W. (2014). Comparative studies on
442 ionospheric climatological features of NmF2 among the Arctic and Antarctic stations. Journal
443 of Atmospheric and Solar-Terrestrial Physics, 119, 63-70.

444 Yamazaki, Y., Kosch, M. J., & Sutton, E. K. (2015), North‐south asymmetry of the
445 high‐latitude thermospheric density: IMF BY effect. *Geophysical Research Letters*, *42*(2),
446 225-232, doi:10.1002/2014GL062748.

Yu, C., Zhang, X.-X., Wang, W., & He, F. (2021). Longitudinal dependence of ionospheric Poynting flux in the Northern Hemisphere during quite times. *Journal of Geophysical Research: Space Physics,* 126, e2021JA029717. https://doi.org/10.1029/2021JA029717